Title

Winter orographic precipitation ratios in the Sierra Nevada - Large-scale atmospheric circulations and hydrologic consequences

Journal

Journal of Hydrometeorology, 5(6)

ISSN

1525-755X

Authors

Dettinger, Michael
Redmond, K
Cayan, D

Publication Date

2004-12-01

Peer reviewed

Winter Orographic Precipitation Ratios in the Sierra Nevada—Large-Scale Atmospheric Circulations and Hydrologic Consequences

MICHAEL DETTINGER

U.S. Geological Survey, Scripps Institution of Oceanography, La Jolla, California

KELLY REDMOND

Western Regional Climate Center, Desert Research Institute, Reno, Nevada

DANIEL CAYAN

U.S. Geological Survey, Scripps Institution of Oceanography, La Jolla, California

(Manuscript received 30 January 2004, in final form 24 May 2004)

ABSTRACT

The extent to which winter precipitation is orographically enhanced within the Sierra Nevada of California varies from storm to storm, and season to season, from occasions when precipitation rates at low and high altitudes are almost the same to instances when precipitation rates at middle elevations (considered here) can be as much as 30 times more than at the base of the range. Analyses of large-scale conditions associated with orographic precipitation variations during storms and seasons from 1954 to 1999 show that strongly orographic storms most commonly have winds that transport water vapor across the range from a more nearly westerly direction than during less orographic storms and than during the largest overall storms, and generally the strongly orographic storms are less convectively stable. Strongly orographic conditions often follow heavy precipitation events because both of these wind conditions are present in midlatitude cyclones that form the cores of many Sierra Nevada storms. Storms during La Niña winters tend to yield larger orographic ratios (ORs) than do those during El Niños. A simple experiment with a model of streamflows from a river basin draining the central Sierra Nevada indicates that, for a fixed overall basin-precipitation amount, a decrease in OR contributes to larger winter flood peaks and smaller springtime flows, and thus to an overall hastening of the runoff season.

1. Introduction

About three-quarters of western U.S. water supplies are derived from high-altitude watersheds, where orographic precipitation from large-scale winter storms is the major contributor (Chang et al. 1987). On average, precipitation on higher-altitude areas is enhanced compared to that on low-lying surroundings as moist air masses are lifted by mountain landforms. However, the extent to which high-altitude catchments receive more precipitation than adjacent low-altitude areas varies from storm to storm, and from year to year, from occasions during which nearly equal amounts of precipitation fall at high and low altitudes to occasions when 10 or more times as much precipitation falls at the higher altitudes. These differences in precipitation distribution may have important implications for land and water resources in the region (as will be illustrated herein) and may be subject to modulations by multiyear climatic fluctuations like El Niño–Southern Oscillation (ENSO; Allan et al. 1996) air–sea interaction of the tropical Pacific and its multidecadal counterpart, the Pacific decadal oscillation (PDO; Mantua et al. 1997). Such modulation presumably would be accomplished by changes in regional atmospheric circulation conditions associated with these large-scale climatic processes. If so, and if those circulation changes can be identified and predicted, then it may be possible to predict variations in orographic precipitation well in advance. It may even be possible to project the future of orographic precipitation enhancements under global-warming scenarios.

The objective of the present study, then, was to identify and quantify large-scale atmospheric conditions associated with variations in orographic precipitation on—as a test case—the windward (western) slopes of the central Sierra Nevada (Fig. 1). Work presented here expands upon previous regional-scale diagnostic efforts by Reece and Aguado (1992), Aguado et al. (1993), and Pandey et al. (1999), and corroborates (locally) the relations between orographic precipitation and mountain-

Corresponding author address: Michael Dettinger, U.S. Geological Survey, Scripps Institution of Oceanography, Dept. 0224, 9500 Gilman Drive, La Jolla, CA 92093-0224.
E-mail: mdettinger@ucsd.edu

FIG. 1. Locations of weather stations used to estimate daily to seasonal orographic precipitation gradients in the central Sierra Nevada; red stars indicate high-altitude stations, and yellow stars indicate low-altitute stations (see Table 1 for details). Blue curve is the trace of the North Fork American River.

slope orientations used in several simplified precipitation models (Rhea and Grant 1974; Colton 1976; Alpert 1986; Hay and McCabe 1998; Pandey et al. 2000). These previous studies have shown the importance of wind directions, relative to the topography of a mountain range, in determining orographic precipitation amounts and distributions, but have neither addressed the long-term historical variations of orographic precipitation nor the influences of interannual climate variations like ENSO and PDO. Previous studies also have not specifically addressed streamflow responses associated with variations in orographic precipitation patterns. The present study characterizes long-term characteristics of orographic precipitation variations in the central Sierra Nevada, with the aim of better understanding its long-term storm-to-storm and year-to-year fluctuations and relations to ENSO, as well as its hydrologic consequences for a river basin typical of the range.

2. Data

In order to characterize short- to long-term fluctuations of these orographic gradients in the central Sierra Nevada of California, a local orographic ratio (OR) index was formed by computing (for all days with at least some precipitation measured in both altitude zones) the ratio of the average of precipitation measured at three weather stations on the western slope of the range to the average at three stations near sea level in the Central Valley (Fig. 1; Table 1). This ratio measures the local enhancement in precipitation that occurs (typically) from stations near the foot of the mountain range to

TABLE 1. Locations and altitudes of weather stations used to estimate orographic-precipitation gradients in the central Sierra Nevada.

Symbol on Fig. 1	Station	Alt (m)	Lat	Lon
		Low-altitude stations		
1	Marysville	21	39°09′N	121°35′W
2	Sacramento	0	38°31′N	121°25′W
3	Stockton	10	37°54′N	121°15′W
		High-altitude stations		
4	Bowman Lake	1555	39°27′N	120°39′W
5	Central Sierra Snow Laboratory	2200	39°19′N	120°22′W
6	Yosemite Park Headquarters	1300	37°45′N	119°35′W

stations a kilometer or two higher and about 100 km farther to the east. The stations were chosen for their long and largely unbroken daily precipitation records, for their locations paralleling the range front near the American River (Fig. 1), and for their altitudes. The low-altitude stations were among the longest term of the near–sea level weather stations in this area, and the high-altitude sites were several of the longest-term stations at highest available altitudes, on the west slope of the range.

Ideally, more stations could be included in the averages in order to further reduce the effects of very local rain shadowing differences from site to site and to station-specific conditions and errors. However, averaging for a single OR index should be restricted to stations on parts of the range front that face more or less in the same directions. Mixing stations from areas of the range that face, for example, southwestward with stations from areas that face due westward would mix their respective uplift influences and muddy the diagnosis of conditions favoring or disfavoring orographic precipitation. The high-altitude stations used in OR were selected because they were among the highest long-term stations on this part (and face) of the Sierra Nevada, and they lie about halfway up the western slope in both altitude (Jeton et al. 1996) and eastward distance. For hydrologic applications of OR, this halfway location might actually be preferred to stations even higher in the range (if they exist) because, with it, OR measures precipitation near the center of the river basins, draining the range rather than measuring it at the farthest extremities of the basins. Furthermore, Neiman et al. (2002) have shown that the height of the low-level jets in landfalling storms in California's Coast Ranges exerts considerable control as to where orographic precipitation reaches its maxima, and these heights typically are well below 850 hPa and well below the highest altitudes in the Sierra Nevada.

Although many local processes strongly influence orographic precipitation (e.g., Browning et al. 1975; Neiman et al. 2002; and references therein), the present study focuses on conditions that are reasonably well represented in large-scale and long-term climatic datasets and in current global-scale climate models. This focus means that a number of important influences, like barrier blocking, jets, and even the evolving details of frontal structures, are only distantly accommodated herein; these processes are simply not represented in any but the most local detailed, technically intensive, and often short-term field campaigns [e.g., with weather radar and wind profilers, as in Neiman et al. (2004)]. Spatially detailed observations are required to untangle the complete determinants of orographic precipitation and are a very desirable part of near-term local and regional weather and streamflow forecasting efforts. However, our longer-term and larger-scale objectives to identify long-lead predictive aspects of orographic precipitation enhancements brought us to our current focus on the largest-scale conditions, which can be analyzed consistently over the 50 yr of near-global climate observations, including the National Centers for Environmental Prediction–National Center for Atmospheric Research (NCEP–NCAR) reanalysis I atmospheric dataset (Kalnay et al. 1996)—which is gridded on the same scales as current seasonal climate predictions and climate-change projections—and, as our local ''ground truth,'' radiosonde soundings from Oakland, California, just west of our study area. Profiles of air temperature, water vapor mixing ratios, wind speeds and directions, and geopotential heights were extracted from both datasets. The reanalysis profiles were used to compute daily vertically integrated water vapor transport rates and directions (described in section 4). Moist static energies

$$gz + c_p\theta + Lq$$

were computed in profiles from the Oakland soundings, where g is gravitational acceleration, z is geopotential height, c_p is the heat capacity of air, θ is potential temperature, L is the latent heat of evaporation, and q is water vapor mixing ratio. Vertical differences in moist static energy are used as an index of the stability of the atmosphere to uplift and convection. Daily surface-air temperatures measured at the six sites used to calculate OR, and historical U.S. weather maps, were also analyzed in order to place the daily OR fluctuations into perspective with respect to the passage of cold fronts.

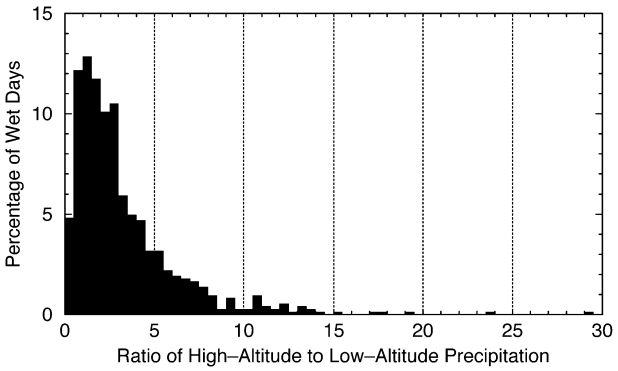

FIG. 2. Distribution of ratios of daily precipitation at high- and low-altitude sites (Table 1) during Dec–Feb 1954–99.

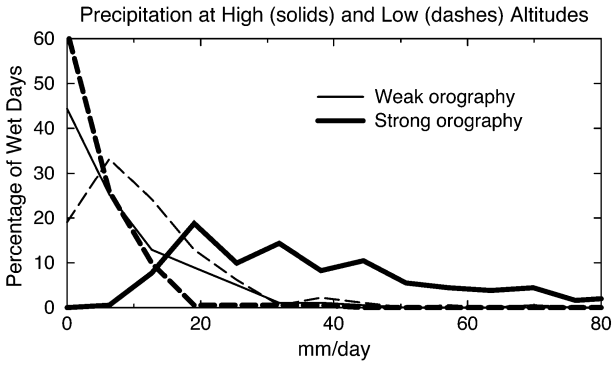

FIG. 3. Distributions of daily precipitation amounts on days with weakly orographic and strongly orographic precipitation ratios, at high and low altitudes, Dec–Feb 1954–99.

3. Variability of orographic precipitation

Daily OR indices were calculated for 723 wet days during Decembers through Februarys from 1954 to 1999. Wet days, constituting about one-sixth of the total winter days during this period, were defined as days averaging more than 2 mm in both the high- and low-altitude stations. The distribution of daily OR values is shown in Fig. 2. On average, 3.3 times as much precipitation falls at the high-altitude sites as at the low-altitude sites, but the precipitation-weighted mean ratio is 4.0, indicating that the wettest days have a (modest) tendency to yield more orographic precipitation enhancement. Daily OR indices range from small fractions to almost 30.

The distributions of the high- and low-precipitation rates during storms with smaller-than-average and larger-than-average, ORs (Fig. 3) indicate that storms differ more in their higher-altitude precipitation rates between large-OR values (strongly orographic storms) and small-OR values (weakly orographic storms) than in their low-altitude rates. Not so obviously from Fig. 3, there is a modest tendency for strongly orographic storms to yield more overall precipitation (averaged over both high- and low-altitude zones). On average, for every centimeter of additional average precipitation, OR increases by about 0.6, but this relation only describes about 10% of the variance of OR.

Seasonal OR indices, computed from total precipitation accumulations at the low- and high-altitude stations during winters (December through February), from 1953 to 1999 are shown in Fig. 4. Winter ORs average about 3, but, in some years, the ratio drops to as low as 1 (as in 1991) or rises to as much as 4 or 5 (as in 1959 and 1999).

4. Atmospheric profiles and circulations

These variations in OR occur in response to differences in storm-time atmospheric conditions. Throughout this paper, various weather conditions on the 25% of all days with measured precipitation at both the low-altitude and high-altitude sites with the largest OR values (totaling 181 cases) are compared to conditions on an equal number of wet days with the lowest OR values; these are the upper- and lower-OR quartiles, respectively. By compositing winds, temperatures, and humidities at various levels in the atmosphere from a 2.5° latitude × 2.5° longitude NCEP–NCAR reanalysis grid cell over northern California, averaging values on the storm days in the upper-OR quartile separately from those in the lower-OR quartile, the average vertical profiles of atmospheric conditions associated with the two types of storms can be determined (heavy curves; Figs. 5a–c). The corresponding profiles from the Oakland radiosonde record confirm the qualitative aspects of the reanalysis-based result reasonably well (light curves; Figs. 5a–c). The profiles show that 1) the average eastward components of winds in the large-OR storms are stronger at all levels than those during small-OR storms, 2) the winds during large-OR storms are more humid at most levels, and 3) temperatures are—on average—

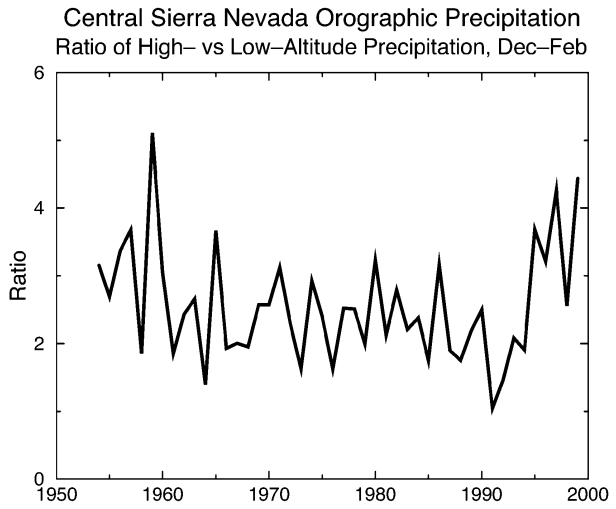

FIG. 4. Ratios of high- to low-altitude Dec–Feb precipitation totals, 1954–99.

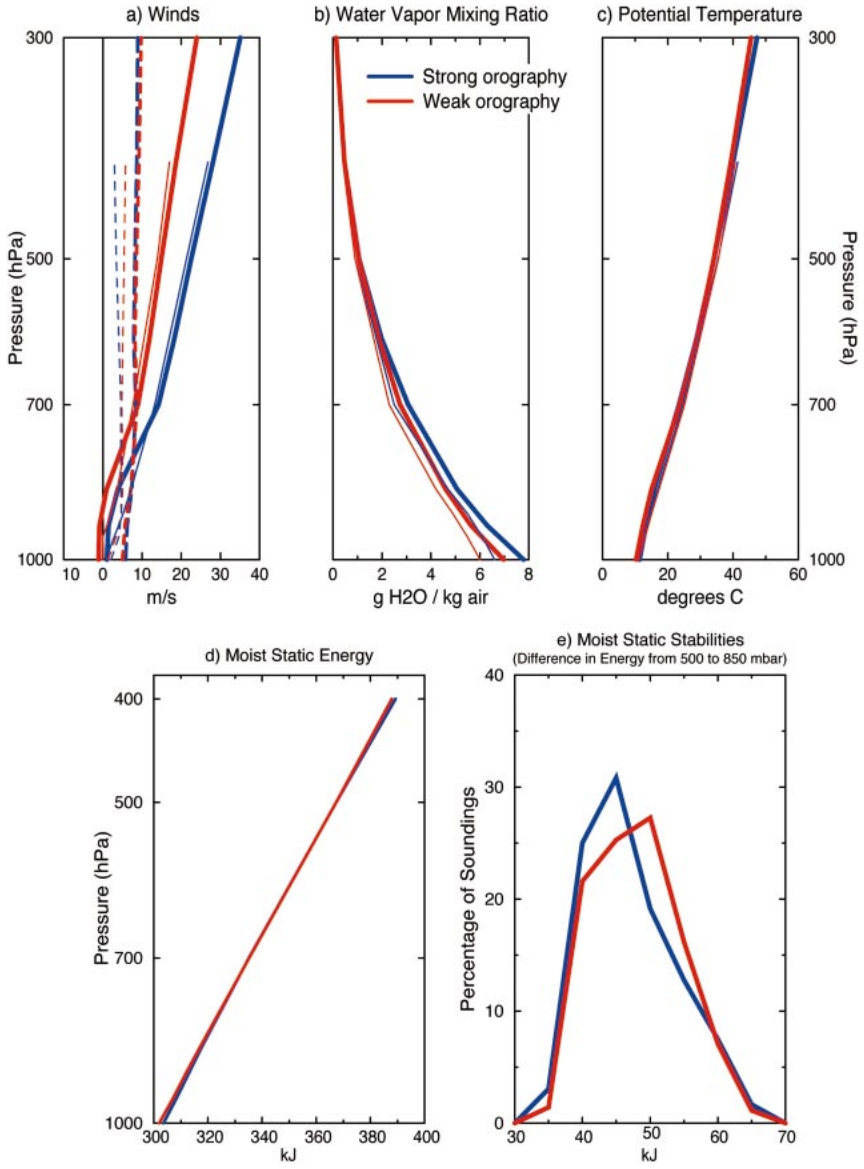

FIG. 5. (a)–(d) Average atmospheric profiles of wind speeds (west–east, solid; south–north, dashed), water vapor mixing ratios, potential temperatures, and moist static energies, for storms with orographic precipitation ratios in the upper quartile (blue) and lower quartile (red) of Dec–Feb storms, 1954–99; heavy curves in (a)–(c) are from NCEP–NCAR reanalysis, and light curves are from radiosonde soundings at Oakland. Both curves in (d) are from Oakland. (e) Distribution of differences between moist static energy at 500 and 850 hPa in soundings at Oakland during days in the upper-OR quartile (blue) and lower-OR (red) quartile.

slightly warmer (<1°C below 500 hPa) in large-OR storms than in small-OR storms.

The average profiles of moist static energy (Fig. 5d) indicate that, on average, the atmospheric profiles during large-OR storms are less stable than during small-OR storms, having a smaller difference between the energies at 850 hPa than at 500 hPa in the large-OR storms. Despite considerable overlap in the distributions of those 500- versus 850-hPa static-energy differences (Fig. 5e), large-OR ratios develop more often when the atmosphere is less stable than when the atmosphere is more stable. Case studies have shown that a less stable profile increases the opportunities for more directly up-and-over wind trajectories to develop, reduces the chances for—and strength of—range-front blocking and along-range jets, and also may allow convective enhancement of precipitation once topographic uplift of the air masses begins (Browning et al. 1975; Peterson et al. 1991; Neiman et al. 2002)

Although atmospheric stability undoubtedly plays an

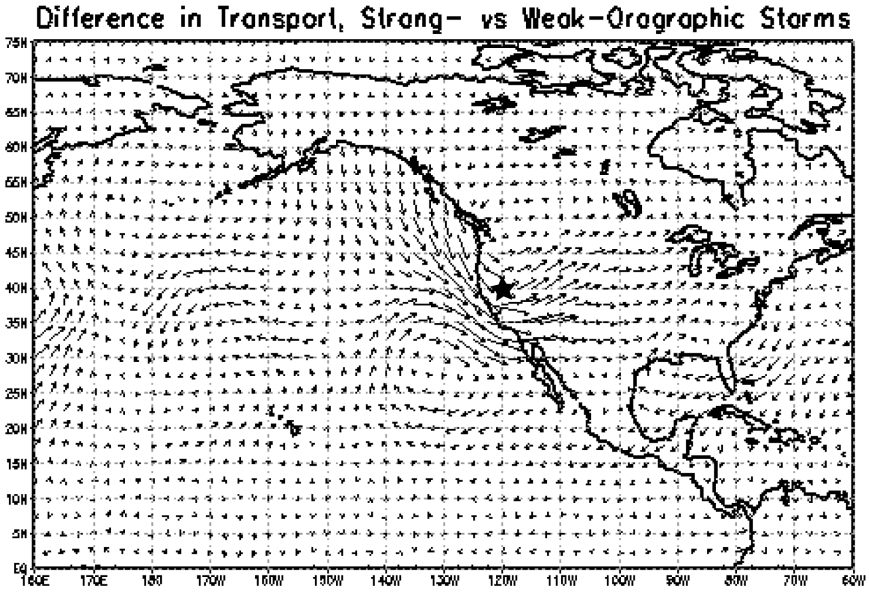

FIG. 6. Vertically integrated water vapor transport differences (on average) between Dec–Feb days with orographic ratios in the upper quartile and the lower quartile, 1954–99. Length of vector proportional to magnitude of (anomalous) transport and head indicates direction toward which transport proceeds; star indicates central Sierra Nevada.

important role in establishing orographic precipitation patterns, the clearest differences between the large-OR and small-OR profiles are in their wind fields. To characterize these differences more completely, daily vertically integrated water vapor transport directions and rates were analyzed. No obviously ''special'' atmospheric levels—where such differences are focused—are observed in the large-scale data sources for Fig. 5, and therefore vertically integrated transports (capturing the essence of both the wind and humidity profiles) are a useful characterization of large-scale atmospheric circulations that affect OR. Vertically integrated vapor-transport vectors were calculated—from the NCEP–NCAR reanalysis fields—by integrating the products $q \times u \times dp/g$ and $q \times v \times dp/g$—where q is water vapor mixing ratio, u is the west–east wind, v is south–north wind, dp is the differential pressure (vertical distance measured in terms of atmospheric pressure), and g is gravitational acceleration—from the earth's surface to the 300-hPa pressure level, at each grid point, at 6-h intervals, and then summing to form the daily eastward transport component, $\langle qu \rangle$, and northward component, $\langle qv \rangle$. (Weighting by dp/g ensures that the transports are weighted by the mass of water at each level.) The resulting vectors represent the daily rates and directions of overall vapor transport above each grid point. The vectors can be averaged to identify large-scale atmospheric circulation patterns that are, on average, associated with various storm types and climatic conditions. The transport vectors have the advantages (a) that by using them, locally over the Sierra Nevada region, the statistical distributions of atmospheric circulations associated with all large- and small-OR storms can be analyzed in more (statistical) detail than is possible with the more commonly used geopotential heights, and (b) that no particular pressure level needs to be specified as the focus of study. Thus, (a) the following analysis is not restricted to means or other measures of central tendencies, and (b) storm-to-storm differences in the atmospheric profiles of vapor transport are naturally accommodated.

To visualize the differences in atmospheric circulations associated with large- and small-OR storms, consider first the anomalous-transport fields obtained by subtracting averages of the $\langle qu \rangle$'s and $\langle qv \rangle$'s from all wet days in the upper-OR quartile from those in the lower-OR quartile (Fig. 6). The largest transport differences are indicated over the West Coast of the United States, where a cyclonic whorl of anomalous transports brings vapor southeastward along the northwest coast and then almost due eastward into the central Sierra Nevada. Overall, vapor is transported toward the range more from the northeast Pacific rather than the subtropical Pacific during the high-OR storms.

The transport pattern in Fig. 6 contrasts with the anomalous transports obtained by subtracting average transports during the days in the overall-wettest quartile and subtracting from those in the lowest quartile (Fig. 7). The pattern is broadly similar, but has anomalous transport into the central Sierra Nevada from a more southwesterly direction (Pandey et al. 1999) and forms a whorl that is centered offshore, rather than inland over eastern Washington as in Fig. 6. The centers of these whorls represent the locations of low pressure anoma-

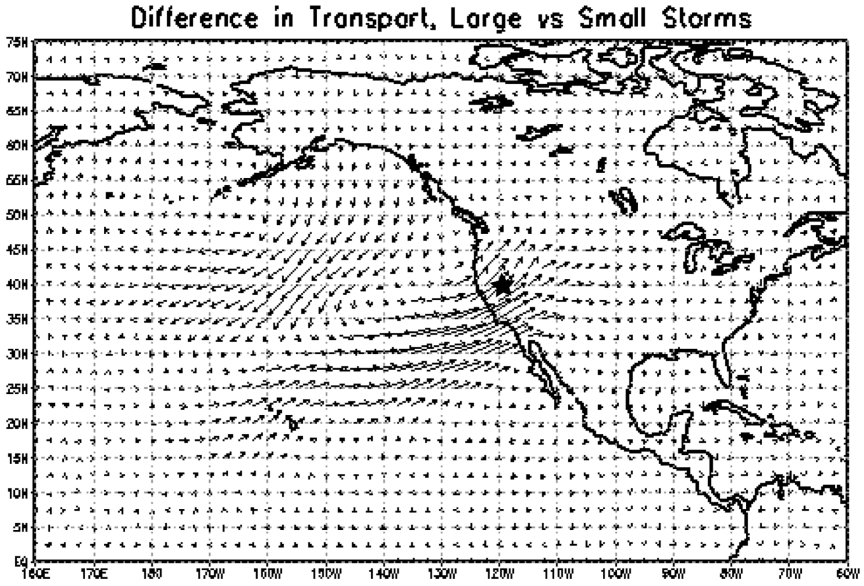

FIG. 7. Same as Fig. 6, except for the differences between large (precipitation total) storms and small storms.

lies, and, indeed, if similar composites (or correlations) were made with 700-hPa heights (not shown), the characteristic pressure patterns associated with large-OR storms, and with large storms, are distinguished mostly by whether the primary low pressure anomalies are located over Washington or offshore.

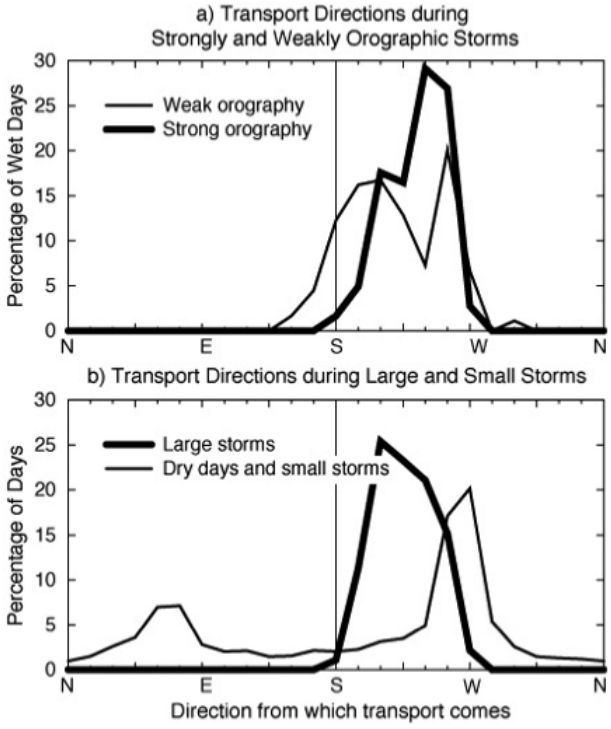

FIG. 8. Distributions of vertically integrated water vapor transport directions associated with storms that are (a) weakly or strongly orographic, and (b) large or small storms to dry days.

The full distributions of transport-vector directions at the reanalysis grid cell immediately west of the central Sierra Nevada for the large-OR storms and small-OR storms are shown in Fig. 8a; corresponding distributions for large and small storms are shown in Fig. 8b. The distribution of transport directions during large-OR storms is more narrowly peaked than the distribution for small-OR storms, and peaks with winds from about 60° west of southerly (note that the distributions in Fig. 8 are of actual transport directions rather than anomalous directions). The distribution of transport directions associated with small-OR storms peaks with winds from roughly south-southeast and (less often) from slightly south of westerly.

Notably, the planar slope joining the high- and low-altitude sites that formed the OR index analyzed here (Fig. 1) has a direction of steepest ascent that is about 35° south of westerly. Thus the transport direction that provides the most orographic uplift for inflowing water vapor is the direction that yields the largest OR values for this set of stations. This direction of maximum uplift over the Sierra Nevada also entails vapor transport over parts of California's Coast Ranges prior to arrival at the stations used here (Fig. 1). Consequently, OR ratios may be influenced by rain shadowing from the Coast Ranges, especially shadowing of the low-altitude stations. However, as noted previously (Fig. 3), precipitation totals at the low-altitude stations differ less—in both absolute and relative terms—from large-OR storms to small-OR storms than do precipitation totals at the high-altitude stations. Furthermore, when the calculations for Fig. 6

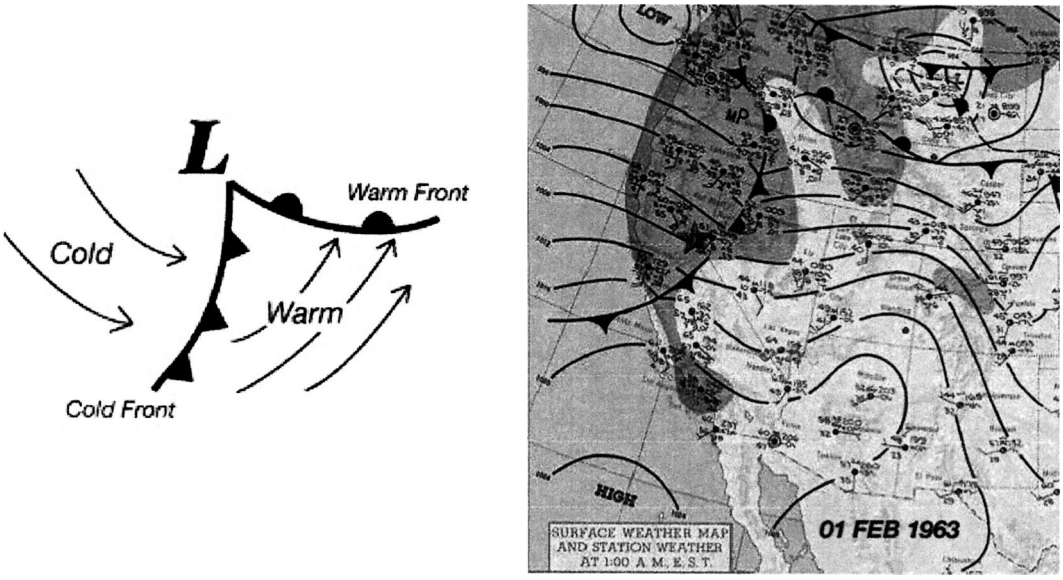

FIG. 9. (left) Idealized structure and (right) a historical example of a midlatitude low pressure cyclone, showing low pressure center (''L''), wind directions, fronts, and air temperatures (after Carlson 1991); the weather map is for the winter day with the highest OR index, 1 Feb 1963, with a star indicating the central Sierra Nevada [from a National Oceanic and Atmospheric Administration (NOAA) Daily Weather Map, currently available online through the NOAA Central Library Data Imaging Project, http://docs.lib.noaa.gov/rescue/dwm/data_rescue_daily_weather_maps.html].

are repeated using only the days with low-altitude precipitation totals above normal, and then using only days with low-altitude precipitation totals below normal, the same anomalous transport patterns across the central California coast and into the central Sierra Nevada are obtained in each calculation. Thus, reductions of precipitation at the low-altitude stations, for example, due to rain shadowing or some other influence, do not control the observed relation between westerly transport direction and large-OR values. That relation seems to have more to do with precipitation and atmospheric conditions at the high-altitude stations than at the low-altitude stations. Other influences certainly affect OR values, like rain shadowing by the Coast Ranges (Andrews et al. 2004), differences in stability of the atmosphere from storm to storm and within storms (Browning et al. 1975), formation of barrier jets (Parish 1982; Neiman et al. 2002), and interactions between the range and the structure of the storms (Neiman et al. 2004), but the first-order large-scale influences appear to be differences in uplift over the range.

As indicated earlier, the transport directions that favor the largest ORs (comparing Fig. 8a to 8b) are not the same as those associated with the largest storms (Pandey et al. 1999). Transport directions associated with large storms are mostly from a more southwesterly direction than are the large-OR storms. The winds from the more southwesterly direction associated with large storms are, on average, warmer and moister than are the more westerly winds associated with large-OR storms, and thus can support larger storm totals (Pandey et al. 1999).

Transport directions on days with most precipitation and those on days with largest OR are significantly different, but they are closely linked in many midlatitude storm systems. The eastward-propagating circulations around many winter low pressure storm systems may be idealized, as in the left panel of Fig. 9, with a sharp cold front where a warm air mass fed by broadly southwesterly winds is undercut by cold air with more westerly and even northwesterly winds. The rapid swing in wind directions associated with the passage of such fronts can quickly substitute cold-sector winds and transports, from westerly directions that favor largest OR values, for the preceding warm-sector transports that arrive from more southwesterly directions, which favor largest overall precipitation totals.

Although many winter storms over California are not well described by the idealization in the left panel of Fig. 9, especially not storms with occluded fronts and more complex forms, the general pattern of winds shown provides a useful conceptual model for the linkages between cold fronts and OR variations in many storms. Visual inspection of the historical daily U.S. weather maps associated with the most extreme OR values revealed that the idealized structure in the left panel of Fig. 9 was clearly recognizable in all of the 20 storms with largest OR values; for example, the right panel of Fig. 9 shows the weather map for the storm with the largest OR value in the time series constructed here. Visual inspection of the weather maps, furthermore, showed that the Sierra Nevada were in the cold sectors of 19 of the 20 largest OR storms. The central Sierra Nevada area was in the warm sector of winter storms, distant from any mapped fronts, or affected by occluded

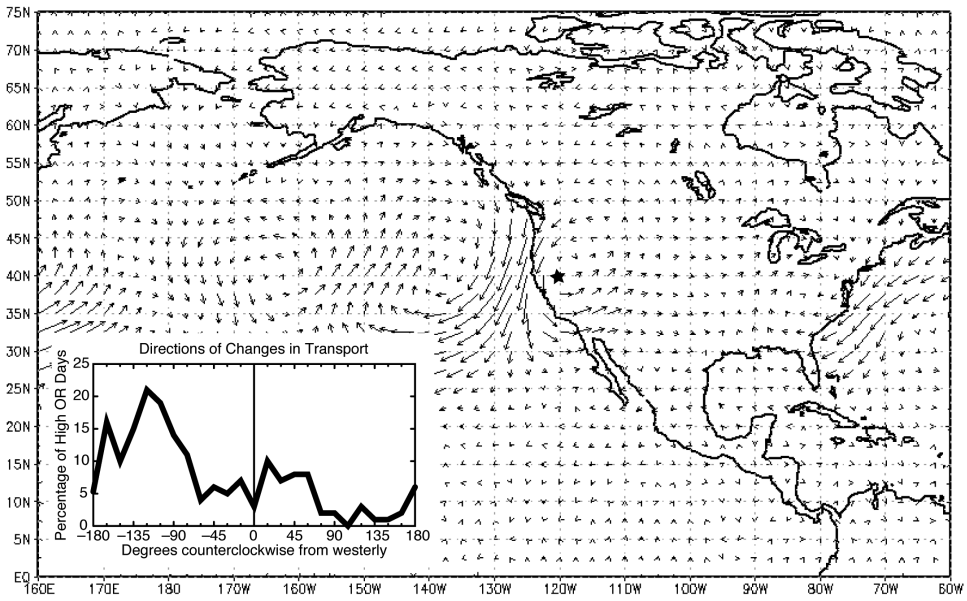

FIG. 10. Same as Fig. 6, except for the differences between days in the upper-OR quartile and the day before; inset shows distribution of directions of change in transport immediately off the California coast (37.5°N, 127.5°W) from the day before to the day of the upper-quartile OR events.

frontal systems in each of the 20 smallest OR storms. The idealized Fig. 9 also was recognizable in the weather maps for each of the 10 overall wettest storms, with the Sierra Nevada in the corresponding warm sector of each storm system. Thus, although many (perhaps, most) winter storms are not as simple as in Fig. 9, its lessons apply well to the largest OR and largest overall storms in the central Sierra Nevada.

The average differences between transports on days in the upper-OR quartile and the immediately preceding day—and the overall distribution of these differences—are shown in Fig. 10. A strong reduction of southerly components of West Coast winds on the days with largest OR from the days immediately preceding is indicated on average. This average reduction reflects the frequent occurrence of changes in transport direction of between about $-135°$ and $-60°$ away from westerly (Fig. 10, inset). Southerly transport components were reduced, from the previous day, on 72% of the days in the upper-OR quartile, and transport vectors rotated more than 45° counterclockwise, from the preceding days, on 88% of the days. Thus, although it is difficult to be exhaustive about the location of fronts on the climatological time scales considered here (as no long-term digital database of front configurations is readily available), wind and transport conditions consistent with the passage of cold fronts are present on a large majority of the 181 days in the upper quartile of OR. Figure 10 also suggests that, although fronts are not well represented in reanalysis fields and global-climate simulations, the effect of cold-front passages on transport directions are reasonably well captured for climatological purposes. Not shown are the transport differences from the days with most overall precipitation to their *following* days, which form a pattern that is nearly the opposite of Fig. 10; this pattern is consistent, in turn, with an association between the wettest days and the passage of warm sectors.

Thus large-OR storms in the central Sierra Nevada are sometimes, and perhaps most often, derived from the cold sectors of winter storms. In the central Sierra Nevada, this association is, in part, due to a propitious orientation of the mountain front. However, orographic precipitation is frequently enhanced in the cold sectors in many mountain settings, despite range orientations (e.g., Browning et al. 1975). The cold air behind midlatitude cold fronts tends to be less convectively stable than the warm air that precedes it (Carlson 1991), and this frequently is true over the central California coast (Fig. 11) and may contribute to the orographic precipitation rates when convection is initiated by orographic uplift (e.g., Neiman et al. 2004).

In keeping with frequent occurrences of these rapid transitions between transports that favor more precipitation to those that favor larger OR, on average, more (total) precipitation falls on the days before days in the upper OR quartile than on the large-OR days themselves. Conversely, on average, OR values are significantly smaller immediately before the highest OR days. More than half of the days in the upper OR quartile are preceded by days in the upper 40% of total wetness; only about one-third of the same high-OR days are this wet. Daily mean temperatures are modestly (but significantly, at $p \sim 0.05$) cooler on the highest OR days than on the day before, and by the day after a high-OR event, temperatures are substantially (-1.5°C) cooler,

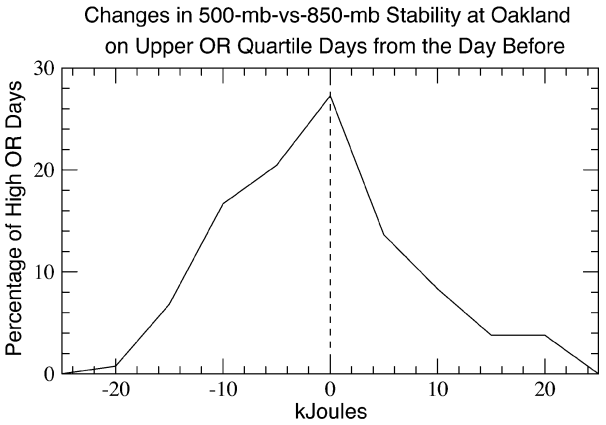

FIG. 11. Distribution of changes in moist static energy differences between 500 and 850 hPa immediately off the California coast (37.5°N, 127.5°W) from the day before to the day of the upper-quartile OR events.

on average. All of these rapid changes immediately before and after the high-OR days are consistent with the frequent occurrence of this sequence of events: (day −1) the warm-air sector east of a cold fronts arrives with southwesterly winds that favor large precipitation totals; (day 0) the passage of the front rapidly brings winds to a westerly or northwesterly direction and introduces less stable conditions, which favor high-OR values; and (day +1) cold air behind the front yields substantial cooling and less total precipitation (but continuing high-OR values). Thus, the passage of low pressure systems and, especially, of cold fronts can strongly and rapidly affect OR and precipitation amounts and may frequently serve to link, and yet separate, days with heaviest precipitation to subsequent days with large-OR values. The association with cold sectors of midlatitude storms is a common aspect of orographic precipitation in many settings (e.g., Browning et al. 1975) due to enhanced instabilities in these sectors, but the association may be enhanced in the central Sierra Nevada where the cold-sector vapor transport directions are often well suited to ensure nearly normal approaches to the range front.

5. Climatic underpinnings

The atmospheric circulations that modulate OR, in turn, may be modulated on interannual time scales by fluctuations of ENSO between its warm tropical El Niño states and its cool tropical La Niña states. The global pattern of regression coefficients describing the variations of the December–February averages of the vertically integrated water vapor transport vectors in response to each degree Celsius of warming (by El Niños) in the equatorial central Pacific is shown in Fig. 12a. The ENSO-induced changes in wintertime transport directions over the northeastern Pacific and West Coast of North America are significant and, on average, El Niño winters yield more anomalously southerly and southwesterly vapor transports into the Sierra Nevada. During La Niña winters, in contrast, transport from the south is diminished. These El Niño–La Niña differences are more commonly identified in the changes (or correlations) of geopotential heights in association with variations of ENSO indices such as the Niño-3.4 sea surface temperature index (Fig. 12b). Negative correlations (associating low pressure anomalies with positive Niño-3.4 deviations) over the northeastern Pacific and southern United States and positive correlations over north-central North America reflect the southward displacement of storm tracks during El Niño winters (with their positive Niño-3.4 indices; Dettinger et al. 2001). The correlations of 700-hPa heights with the seasonal values of OR (Fig. 4), shown in Fig. 12c, are roughly the negative of the correlations with Niño-3.4 (Fig. 12b), with positive correlations, indicating high pressure anomalies over the northern Pacific and southern states, and negative correlations (low pressures) over northwestern North America. Thus on average, as suggested by Fig. 12a, El Niño winters are negatively associated with the atmospheric circulations that favor large-OR values.

These associations of winter-averaged circulations that favor (or disfavor) large values of the particular OR series constructed here with La Niñas (El Niños) are neither exact nor unfailing. For example, the long-term correlation between Niño-3.4 SST and our OR is only $r = -0.20$. However, ENSO relations to OR values can be stronger in some places; for example, correlations between an OR index of Sacramento and Lake Tahoe, California, precipitation rates and another ENSO index (the Southern Oscillation index; Allan et al. 1996) was almost $r = +0.4$. Given the local variations in the ENSO influence on OR, it is worth considering the full distributions of transport directions into the Sierra Nevada during storms in El Niño winters and La Niña winters, as shown in Fig. 13a. Transport directions during storms in La Niña winters are more focused and are focused at more nearly the optimal direction for large-OR values than are transports during storms in El Niño winters. Interestingly, the distribution of transports during El Niños is bimodal, with a peak near the direction favored by large-OR storms (Fig. 8a) and another, equal peak near the direction favored by the overall largest storms (Fig. 8b). As a consequence of these transport-direction distributions, (a) more storms during La Niña winters have had large-OR values, and fewer have had small values, than among the El Niño storms (Fig. 13b), and (b) El Niño winters include more of the largest winter storms than do La Niña winters (not shown). Notably, in other settings in California, the topography is oriented differently from the area considered here, and El Niño circulations are almost ideally situated to generate large-OR values (e.g., in the Coast Ranges near Monterey, California; Andrews et al. 2004).

During El Niño winters, storm tracks tend to cross the West Coast farther south than during La Niña winters

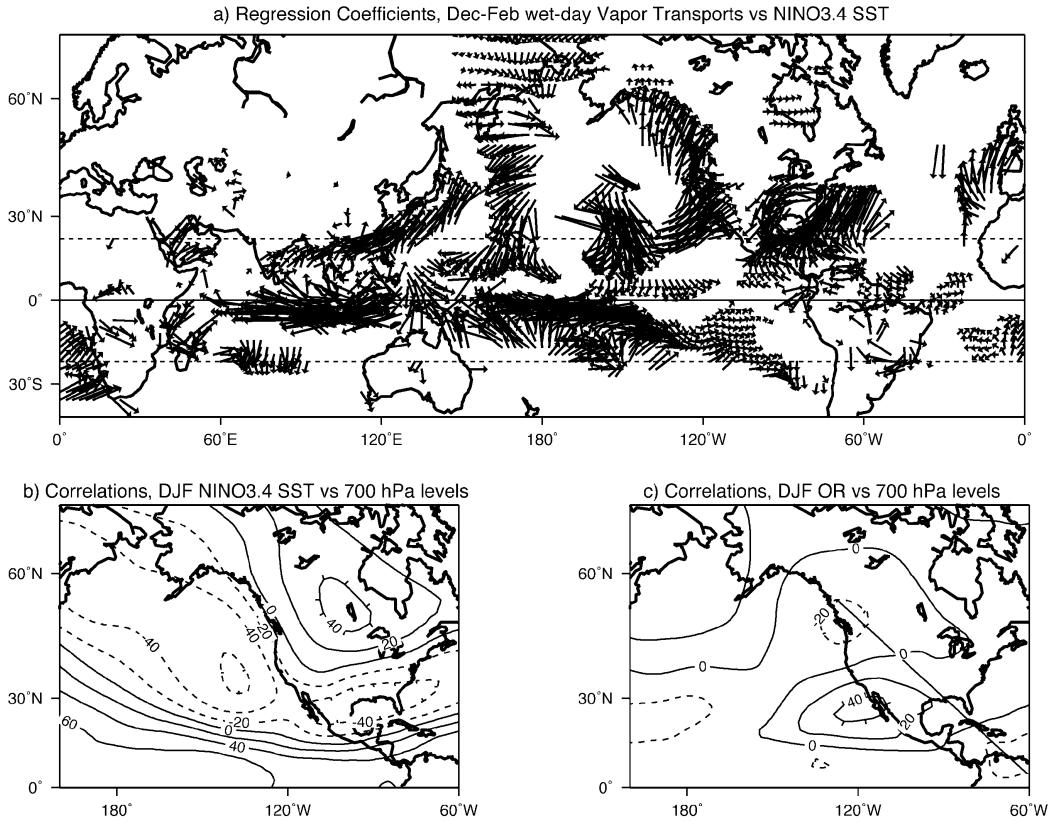

FIG. 12. (a) Regression coefficients relating each 1°C increase in average Dec–Feb SST in the Niño-3.4 region (5°S to 5°N, 120° to 170°W) to Dec–Feb mean water vapor transport vectors during wet days in the central Sierra Nevada, 1950–98; the eastward extent of each vector measures the regression coefficient relating Dec–Feb averages of eastward vapor transport on wet days in the central Sierra Nevada to the corresponding Niño-3.4 SST index; the northward extent of the vector measures the regression coefficient between northward transport and Niño-3.4. Vectors are only mapped if at least one of the regression coefficients is significantly different from zero by a Student's *t* test. (b), (c) Correlations of Dec–Feb mean 700-hPa heights with the Niño–3.4 SST index and winter-mean OR for the central Sierra Nevada, respectively.

(Dettinger et al. 2001). The southward displacement of storm tracks during El Niño winters brings the storm centers (like the idealized cyclone of Fig. 9) southward toward the Sierra Nevada and may explain the bimodal (southwesterly and westerly) distribution of transports associated with El Niño storms (Fig. 13a). The southwesterly and westerly winds around midlatitude cyclones are typically strongest in the parts of the warm and the cold sector nearest the low pressure center, and the southward displacement of the storms may increase the chances that these sectors will impinge upon the range vigorously and in rapid succession. Winter storms often arrive at the West Coast along more zonal paths during El Niño winters (Dettinger et al. 2001). In contrast, during La Niña winters, the storm cores cross the West Coast farther north, and, in many instances, only the cold-front ''tail'' and the westerly winds behind it in the cold sectors reach the Sierra Nevada in force. However, within any given El Niño winter, there is enough scatter between storm tracks and configurations (Yarnal and Diaz 1986) so that storm OR values are not exclusively ''El Niño–like'' or ''La Niña–like.'' Rather, ENSO status only conditions El Niño and La Niña OR distributions that overlap considerably.

On decadal time scales, the anomalous vapor-transport pattern (not shown here) associated with the PDO (Mantua et al. 1997)—like so many other aspects of that interdecadal variation of the North Pacific climate system—closely resembles the corresponding ENSO pattern in Fig. 12a. However, on the multidecadal time scales that characterize fluctuations of the PDO, many different strong ENSO and weak ENSO winters are mixed, and many different storm configurations reach the central Sierra Nevada. Thus, the distributions of transport directions associated with the positive (El Niño–like) and negative (La Niña–like) phases of PDO are not as distinct (Fig. 14a) as were the corresponding distributions with ENSO (Fig. 13a). Fewer storms during the negative PDO phases have southerly transports than in the positive PDO phase, and relatively more (about 5%) yield transports optimal for large-OR values. The result is a small overall increase in the number of

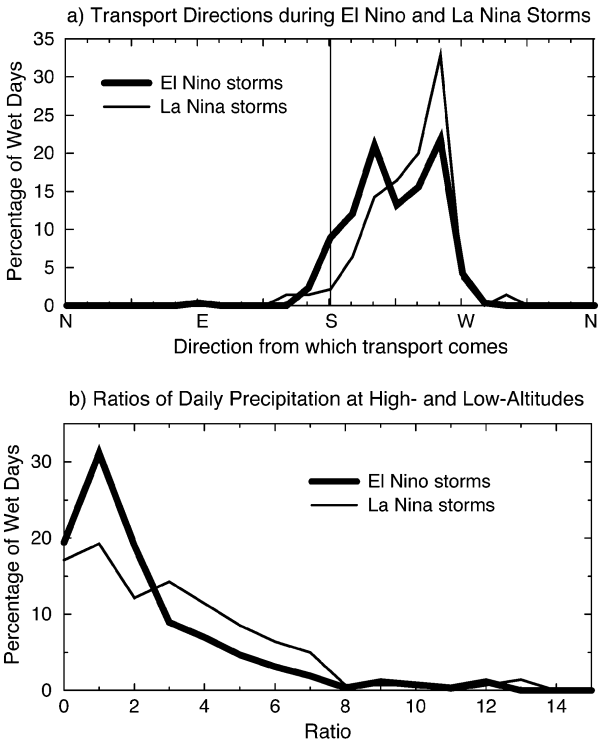

FIG. 13. Distributions of (a) water vapor transport directions and (b) orographic precipitation ratios associated with storms during El Niño and La Niña winters, 1954–99.

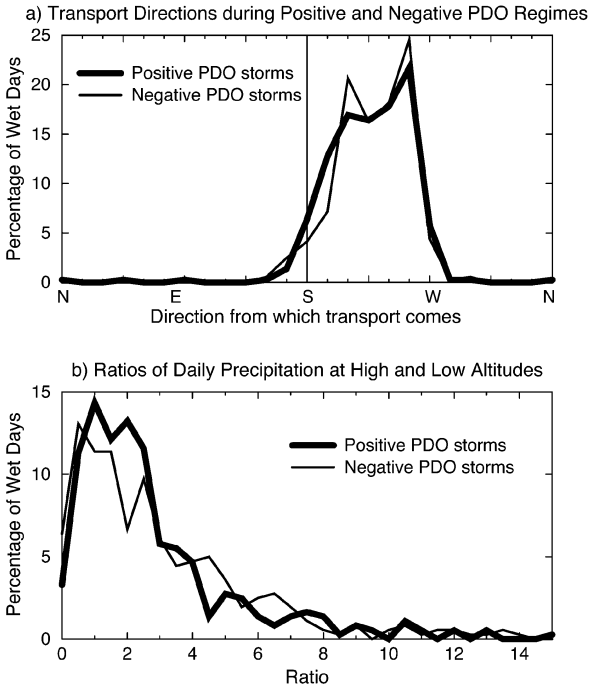

FIG. 14. Distributions of (a) water vapor transport directions and (b) orographic precipitation ratios associated with storms during positive- and negative-PDO winters, 1954–99.

large-OR storms, and a decrease in the number of small-OR storms, during negative PDO regimes compared to positive PDO regimes (Fig. 14b).

6. Hydrologic consequences

Variations in OR, from storm to storm and from season to season, have the potential to significantly influence the quantity and timing of water supplies from the central Sierra Nevada, and analogous variations of the strength of orographic precipitation gradients in other mountain ranges may exert similar influences on most western rivers. When disproportionately little precipitation is deposited at high altitudes (small-OR conditions), even a ''wet'' year may yield less of the crucial warm-season snowmelt runoff than expected. Conversely, the added high-altitude precipitation and snowpack associated with large-OR winters will yield more discharge when the snowpack finally begins to melt. Flood generation by winter storms also depends on their OR values, with warm-storm floods being aggravated when the storms have larger-OR values so that they provide more precipitation as rain at middle and higher altitudes. Recall that, on average, high-OR storms are somewhat warmer than storms with very low OR values; this results in storm-time snow lines (on the surface) that are 150–300 m higher during high-OR storms. Cool-storm floods are dependent on abundant low-altitude rains so that lower-OR values (for a given total precipitation amount) can aggravate them.

This general set of hydrologic consequences can be illustrated succinctly with simulations of streamflow responses to prescribed (hypothetical) changes in orographic precipitation in watershed models with enough spatial detail to represent elevational differences in precipitation amounts, precipitation form (rain or snow), and snowmelt rates. Thus, as an illustration of the influence of OR on streamflow in the Sierra Nevada, a detailed watershed model of the North Fork American River above Sacramento (Fig. 1), developed and calibrated by Jeton et al. (1996), was used to simulate streamflow differences during January through September of 1983, under three specified OR regimes.

The North Fork American River drains a basin that spans the full range of altitudes of the western slope of the Sierra Nevada, in the midst of the stations used to calculate the OR time series considered here (Fig. 1). The North Fork American River watershed model uses the Precipitation-Runoff Modeling System (Leavesley and Stannard 1995) and represents spatial variations of topography, climate, vegetation, and soils that are 100 m or larger in terms of ''pixelated'' hydrologic response units (HRUs; Jeton and Smith 1993). The model simulates streamflow generation by rainfall and snowmelt runoff over the land surfaces and through the subsurface, on daily time steps, in response to daily precipitation totals and maximum and minimum temperatures at four long-term weather stations at altitudes ranging

from 700 to 2100 m above sea level. The model has been used previously to hindcast and forecast streamflow from days to months in the future (Dettinger 1997; Dettinger et al. 1998, 1999; Miller et al. 1999) and to estimate climate-change responses (Jeton et al. 1996; Miller et al. 2001; Wilby and Dettinger 2000).

In the American River model, each HRU receives the same daily precipitation as was measured at the weather station closest in elevation to it. For simulations of the effect of orographic precipitation gradients on streamflow, it was necessary to adjust the daily station precipitation rates to reflect the desired changes in the precipitation gradients while maintaining the simulation-period basin-total precipitation at its observed value. An adjustment factor for the daily precipitation inputs from each station was derived by fitting a regression relation between precipitation totals for 1983 at each station and the elevations of the stations, to obtain

$$P_i = C + bE_i, \tag{1}$$

where P_i is the annual total (or average) precipitation at station i; E_i is the elevation there; C is the fitted intercept; and b is the slope of the regression line. For the simulations with alternative orographic precipitation gradients, we required that a new (hypothetical) set of precipitation rates, P'_i, equal

$$P'_i = C' + kbE_i, \tag{2}$$

where C' is a new constant (required to maintain the observed basin-total precipitation rate), and k multiplies b to adjust the orographic precipitation gradient as desired. The multiplier k is specified, which leaves C' to be determined from the constraint that basin-total precipitation is not changed,

$$\langle A_i P_i \rangle = \langle A_i P'_i \rangle, \tag{3}$$

where brackets $\langle\ \rangle$ indicate totalling over the basin, and A_i is the area within the basin that receives P_i. Solving for C' in Eqs. (1) to (3), and then substituting back into Eq. (2), yields

$$P'_i = \langle A_i P_i \rangle / \langle A_i \rangle - kb\langle A_i E_i \rangle / \langle A_i \rangle + kbE_i. \tag{4}$$

This equation describes the adjustments to the annual precipitation totals at each station, but on a daily basis, a multiplier is preferable (e.g., so that dry days remain dry). Thus, from Eq. (4), we derived multipliers γ_i of daily precipitation values at each station that ensure that the total P'_i at the station, determined from Eq. (4), would equal $\gamma_i P_i$. The multipliers γ_i that accomplish this are

$$\gamma_i = \langle A_i P_i \rangle / \langle A_i \rangle P_i - kb\langle A_i E_i \rangle / \langle A_i \rangle P_i + kbE_i / P_i. \tag{5}$$

A multiplier is thereby determined for each of the weather stations, depending on the desired OR adjustment k, on the observed P_i totals for 1983, and on the regression coefficient b fitted to total P_i and E_i. Then all daily precipitation values were multiplied by the γ_i's for each simulation described here.

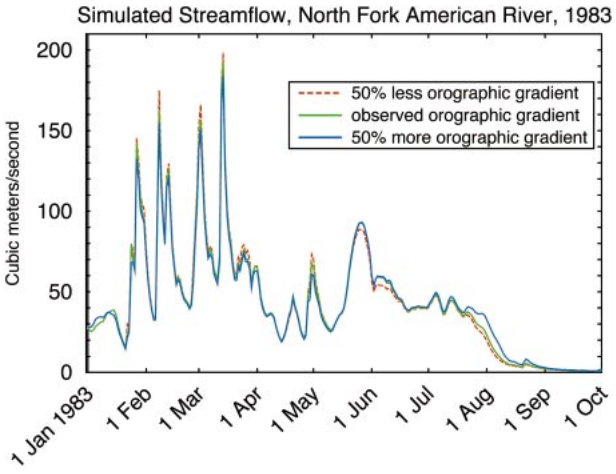

FIG. 15. Simulated streamflow hydrographs for the North Fork American River, Jan–Sep 1983, with observed precipitation patterns and patterns adjusted to maintain the same total amounts but with an artificially imposed 50% increase in orographic precipitation gradient and a 50% decrease in orographic precipitation gradient.

Streamflow was simulated in response to 1) $k = 1$, the case where observed 1983 daily distributions of temperature and precipitation were applied; 2) $k = 1.5$, a hypothetical precipitation distribution with the basin-total precipitation the same as observed, but with the average orographic gradient increased by 50% (making ORs uniformly larger), and 3) $k = 0.5$, a hypothetical precipitation distribution with the precipitation total the same, but with the gradient decreased by 50% (making ORs uniformly smaller). Temperature inputs and all other variables and parameters were not changed from simulation to simulation.

In response to these changes in the spatial distributions, but not overall amounts, of precipitation, streamflow flood peaks caused by winter storms (which continued into May that year) increased by 15% when OR was reduced, and streamflow during the April–July snowmelt decreased by about 10% (Fig. 15). Although temperatures were not changed from simulation to simulation, the larger OR ($k = 1.5$) precipitation distribution provides less precipitation at lower altitudes than did the small OR ($k = 0.5$) distribution. Because much of the missing precipitation at the lower altitudes would have been delivered as rainfall or as short-lived snow, less runoff was generated from rainfall and storm-time snowmelt in the large-OR simulation. Consequently, winter flood peaks were smaller. More precipitation—typically as snowfall—was delivered at the higher altitudes, so proportionally more of the precipitation input to the basin was stored in high-altitude snowfields. Consequently, spring and summer snowmelt runoff from the high altitudes was larger and lasted longer. The effects of the small-OR precipitation distribution on rainfall, snowmelt, flooding, and warm-season runoff were just the opposite.

Together, the increases in winter runoff and decreases

in spring runoff yield an earlier overall runoff regime under the small-OR conditions, with the day of year by which half the year's runoff has passed coming a full week earlier. Similar results were obtained from simulations (not shown) of streamflow responses to similarly specified OR changes in a model of the upper Merced River basin (Wilby and Dettinger 2000), above Yosemite Valley (Fig. 1), and from simulations of both rivers in years other than 1983. The North Fork American River, in 1983, yields especially large responses to OR changes (i) because the American River model represents a more balanced mix of high and low altitudes (and precipitation rates) than does the upper Merced River model, which is almost entirely above 2000 m above sea level, and (ii) because 1983 had an especially long wet season, which accentuated the different runoff responses of the low and high parts of the basins. Both of these factors heighten the effects of OR change.

This simulated hastening of runoff timing in Fig. 15 is in the same sense as, and is of comparable magnitude to, observed trends in western North American runoff timing during recent decades (Cayan et al. 2001). The observed timing trends have been ascribed mostly to long-term warming of winters and springs (Cayan et al. 2001). The possible role of OR variations in causing the observed timing trends needs more attention, because, even with no change in temperatures or in overall precipitation amounts and timing, runoff timing can be changed by OR variations alone. In the present study, no long-term trend in OR of the duration or magnitude needed to explain recent interdecadal runoff timing trends is evident (Fig. 4). However, other studies have argued that long-term historical changes in the orographic gradients should be, and probably are, present (Rosenfeld 2000; Rosenfeld et al. 2003), due to local influences of air pollution on winter storms. If OR is changing systematically in parts of the Sierra Nevada and other western mountain ranges, those changes would certainly complicate interpretations of recent streamflow-timing trends in the Sierra Nevada.

7. Summary

The extent to which winter precipitation is orographically enhanced as one moves up into the Sierra Nevada varies from storm to storm, and season to season, from occasions when there is little difference between high- and low-altitude precipitation rates to instances when precipitation rates at middle elevations (considered here) can be as much as 30 times larger than at the base of the range. Many local-scale processes strongly affect orographic precipitation; these processes are typically not recorded in large-scale or long-term climatic datasets, nor are they simulated in the large-scale models used for seasonal climate forecasts or climate-change projections. In order to better interpret the longer history of orographic precipitation patterns, and to prepare for predictions of future changes in those patterns, this study investigated large-scale atmospheric conditions from long-term climatic datasets to explore associations with orographic precipitation in the central Sierra Nevada area.

Strongly orographic storms most commonly have winds that transport water vapor across the range from a nearly westerly direction, which contrasts with wind directions associated with the overall wettest storms. The atmosphere is also less convectively stable during highly orographic storms; however, this association is not as distinct as is the influence of transport directions. Strongly orographic conditions often follow heavy precipitation events because they are present in the warm and cold sectors, respectively, of midlatitude cyclones that form the cores of many wintertime storms in the Sierra Nevada. La Niña winters have yielded more storms with large orographic ratios (ORs) than have El Niños winters. Winters during negative (La Niña–like) PDO winters tend to yield slightly more storms with large ORs than do positive-PDO winters. No long-term trends are detected in the particular OR series studied here.

A simple experiment with a watershed model of the North Fork American River shows that, for a fixed basin-total precipitation amount, a decrease in OR contributes to larger winter flood peaks because more precipitation is deposited (largely as rain) at lower altitudes. A specified reduction of OR also yields smaller springtime flows because less snow is deposited at the highest altitudes. Together these changes demonstrate that streamflow rates and timing from the Sierra Nevada can be influenced by fluctuations of OR, even if temperatures, precipitation amounts, and precipitation timing do not change.

Variations in large-scale atmospheric circulation patterns and transport directions can be used to identify long-term tendencies—when they exist—toward larger- or smaller-OR values. Variations in storm-time atmospheric stability also influence OR values, albeit somewhat less distinctly than do the transport directions. The large-scale circulation differences may be recognizable even in models and predictions that do not contain enough topographic detail, or adequate moist physics, to directly represent the Sierra Nevada topography and orographic precipitation. If the climate processes at work in a particular prediction (e.g., midlatitude cyclones, El Niños, and even global warming) yield reliable projections of changes in atmospheric circulations over the northeast Pacific, in ways that project significantly onto, or away from, the ''preferred'' transport directions for orographic precipitation in the Sierra Nevada, then projections of the future of orographic precipitation might be possible, even using a model with no Sierra Nevada at all.

However, the results presented here describe relations between large-scale atmospheric circulations and orographic precipitation distributions in a rather local setting, centered on a part of the central Sierra Nevada. The results presented here locally confirm simple geometric and stability relations with orographic precipitation that have been used in simple precipitation-in-

terpolation schemes (e.g., Rhea and Grant 1974; Hay and McCabe 1998; Pandey et al. 2000). Further investigation of long-term climate-driven aspects of those relations, extending the present results to additional areas and ranges, would provide a useful avenue for predicting changes in the climatology of OR throughout the region, by allowing OR predictions of considerable spatial detail to be formulated from mountain-slope orientations combined with predicted circulation changes over the northeastern Pacific.

Acknowledgments. This study was funded by the California Energy Commission's California Climate Change Center at Scripps Institution of Oceanography, by NOAA's California Applications Program, and by the Geological Survey's Hydroclimatology and San Francisco Bay Priority Ecosystem Programs.

REFERENCES

Aguado, E., D. Cayan, B. Reece, and L. Riddle, 1993: Patterns of orographic uplift in the Sierra Nevada and their relationship to upper-level atmospheric circulation. *Proc. Ninth Pacific Climate (PACLIM) Workshop,* Pacific Grove, CA, California Department of Water Resources, Interagency Ecological Studies Program Tech. Rep. 34, 153–163.

Allan, R. J., J. Lindesay, and D. Parker, 1996: *El Niño, Southern Oscillation & Climatic Variability.* CSIRO Publishing, 405 pp.

Alpert, P., 1986: Mesoscale indexing of the distribution of orographic precipitation over high mountains. *J. Climate Appl. Meteor.,* **25,** 532–545.

Andrews, E. D., R. C. Antweiler, P. J. Neiman, and F. M. Ralph, 2004: Influence of ENSO on flood frequency along the California coast. *J. Climate,* **17,** 337–348.

Browning, K. A., C. W. Pardoe, and F. F. Hill, 1975: The nature of orographic rain at wintertime cold fronts. *Quart. J. Roy. Meteor. Soc.,* **101,** 333–352.

Carlson, T. N., 1991: *Mid-latitude Weather Systems.* Harper Collins Academic, 507 pp.

Cayan, D. R., S. Kammerdiener, M. D. Dettinger, J. M. Caprio, and D. H. Peterson, 2001: Changes in the onset of spring in the western United States. *Bull. Amer. Meteor. Soc.,* **82,** 399–415.

Chang, A. T. C., J. L. Foster, P. Gloersen, W. J. Campbell, E. G. Josberger, A. Rango, and Z. F. Danes, 1987: Estimating snowpack parameters in the Colorado River basin. *Proc. Large Scale Effects of Seasonal Snow Cover,* Vancouver, BC, Canada, International Union of Geodesy and Geophysics, IAHS Publication 166, 343–353.

Colton, D. E., 1976: Numerical simulation of the orographically induced precipitation distribution for use in hydrologic analyses. *J. Appl. Meteor.,* **15,** 1241–1251.

Dettinger, M. D., 1997: Forecasting runoff pulses in the Merced River, Yosemite Valley, California, springs 1979–97: *Eos, Trans. Amer. Geophys. Union,* **78** (Fall Meeting Suppl.), Abstract H21F-8.

——, K. C. Mo, D. R. Cayan, and D. H. Peterson, 1998: Hindcasts and forecasts of streamflow in the Merced and American Rivers, Sierra Nevada, during recent El Niños. *Eos, Trans. Amer. Geophys. Union,* **79** (Fall Meeting Suppl.), Abstract H22E-06.

——, ——, ——, and A. E. Jeton, 1999: Global to local scale simulations of streamflow in the Merced, American, and Carson Rivers, Sierra Nevada, California. Preprints, *14th Conf. on Hydrology,* Dallas, TX, Amer. Meteor. Soc., 80–82.

——, D. S. Battisti, R. D. Garreaud, G. J. McCabe, and C. M. Bitz, 2001: Interhemispheric effects of interannual and decadal ENSO-like climate variations on the Americas. *Interhemispheric Climate Linkages: Present and Past Climates in the Americas and Their Societal Effects,* V. Markgraf, Ed., Academic Press, 1–16.

Hay, L. E., and G. J. McCabe, 1998: Verification of the Rhea-Orographic-Precipitation model. *J. Amer. Water Resour. Assoc.,* **34,** 103–112.

Jeton, A. E., and J. L. Smith, 1993: Development of watershed models for two Sierra Nevada basins using a Geographic Information System. *Water Resour. Bull.,* **29,** 923–932.

——, M. D. Dettinger, and J. L. Smith, 1996: Potential effects of climate change on streamflow, eastern and western slopes of the Sierra Nevada, California and Nevada. U.S. Geological Survey Water Resources Investigations Rep. 95-4260, 44 pp.

Kalnay, E., and Coauthors, 1996: The NCEP/NCAR 40-Year Reanalysis Project. *Bull. Amer. Meteor. Soc.,* **77,** 437–471.

Leavesley, G. H., and L. G. Stannard, 1995: The precipitation-runoff modeling system—PRMS. *Computer Models of Watershed Hydrology,* V. P. Singh, Ed., Water Resource Publications, 281–310.

Mantua, N. J., S. R. Hare, Y. Zhang, J. M. Wallace, and R. C. Francis, 1997: A Pacific interdecadal climate oscillation with impacts on salmon production. *Bull. Amer. Meteor. Soc.,* **78,** 1069–1079.

Miller, N., J. W. Kim, and M. D. Dettinger, 1999: California streamflow evaluation based on a dynamically downscaled 8-year hindcast (1988–1995), observations, and physically based hydrologic models. *Eos, Trans. Amer. Geophys. Union,* **80** (Fall Meeting Suppl.), Abstract H32G-09.

——, ——, and ——, 2001: Climate change sensitivity analysis of two California headwaters: American River and Russian River: *Proc. 17th Pacific Climate (PACLIM) Workshop,* Santa Catalina Island, CA, California Department of Water Resources, Interagency Ecological Program Rep. 67, 110.

Neiman, P. J., F. M. Ralph, A. B. White, D. E. Kingsmill, and P. O. G. Persson, 2002: The statistical relationship between upslope flow and rainfall in California's coastal mountains—Observations during CALJET. *Mon. Wea. Rev.,* **130,** 1468–1492.

——, P. O. G. Persson, F. M. Ralph, D. P. Jorgensen, A. B. White, and D. E. Kingsmill, 2004: Modification of fronts and precipitation by coastal blocking during an intense landfalling winter storm in southern California: Observations during CALJET. *Mon. Wea. Rev.,* **132,** 242–273.

Pandey, G. R., D. R. Cayan, and K. P. Georgakakos, 1999: Precipitation structure in the Sierra Nevada of California during winter: *J. Geophys. Res.,* **104** (D10), 12 019–12 030.

——, ——, M. D. Dettinger, and K. P. Georgakakos, 2000: A hybrid model for interpolating daily precipitation in the Sierra Nevada of California during winter. *J. Hydrometeor.,* **1,** 491–506.

Parish, T. R., 1982: Barrier winds along the Sierra Nevada Mountains. *J. Appl. Meteor.,* **21,** 925–930.

Peterson, T. C., L. O. Grant, W. R. Cotton, and D. C. Rogers, 1991: The effects of decoupled low-level flow on winter orographic clouds and precipitation in the Yampa River valley. *J. Appl. Meteor.,* **30,** 368–386.

Reece, B., and E. Aguado, 1992: Accumulation and melt characteristics of northeastern Sierra Nevada snowpacks. *Managing Water Resources under Global Change,* H. Raymond, Ed., American Water Resources Association, 631–640.

Rhea, J. O., and L. O. Grant, 1974: Topographic influences on snowfall patterns in mountainous terrain. *Proc. Symp. on Advanced Concepts and Techniques in the Study of Snow and Ice Resources,* Monterey, CA, National Academy of Sciences, 182–192.

Rosenfeld, D., 2000: Suppression of rain and snow by urban and industrial air pollution. *Science,* **287,** 1793–1796.

——, A. Givate, A. Khain, and G. Kelman, 2003: Urban aerosol-induced changes of precipitation. *Eos, Trans. Amer. Geophys. Union,* **84** (Fall Meeting Suppl.), Abstract U51A-02.

Wilby, R. L., and M. D. Dettinger, 2000: Streamflow changes in the Sierra Nevada, California, simulated using statistically downscaled general circulation model output. *Linking Climate Change to Land Surface Change,* S. McLaren and D. Kniveton, Eds., Kluwer Academic, 99–121.

Yarnal, B., and H. F. Diaz, 1986: Relationships between extremes of the Southern Oscillation and the winter climate of the Anglo-American Pacific coast. *J. Climatol.,* **6,** 197–219.